

Three evolutionary paths for magnetar oscillations

K. Glampedakis^{1,2} and D. I. Jones^{3★}

¹*Departamento de Física, Universidad de Murcia, E-30100 Murcia, Spain*

²*Theoretical Astrophysics, University of Tübingen, Auf der Morgenstelle 10, D-72076 Tübingen, Germany*

³*Mathematical Sciences and STAG Research Centre, University of Southampton, Southampton SO17 1BJ, UK*

Accepted 2013 December 30. Received 2013 December 3; in original form 2013 August 2

ABSTRACT

Quasi-periodic oscillations (QPOs) have been seen in the light curves following several magnetar giant flares. These oscillations are of great interest as they probably provide our first ever view of the normal modes of oscillation of neutron stars. The state of the art lies in the study of the oscillations of elastic–magnetic stellar models, mainly with a view to relating the observed frequencies to the structure and composition of the star itself. We advance this programme by considering several new physical mechanisms that are likely to be important for magnetar oscillations. These relate to the superfluid/superconducting nature of the stellar interior and the damping of the modes, both through internal dissipation mechanisms and the launching of waves into the magnetosphere. We make simple order-of-magnitude estimates to show that both the frequencies and the damping time of magnetar oscillations can evolve in time, identifying three distinct ‘pathways’ that can be followed, depending upon the initial magnitude of the mode excitation. These results are interesting as they show that the information buried in magnetar QPOs may be even richer than previously thought, and motivate more careful examination of magnetar light curves, to search for signatures of the different types of evolution that we have identified.

Key words: dense matter – stars: magnetars – stars: neutron – stars: oscillations.

1 INTRODUCTION

Amongst the various known incarnations of neutron stars, a magnetar is undoubtedly one of the most extreme. These objects are believed to be endowed with the strongest magnetic fields in nature, somewhere in the range of 10^{14} – 10^{15} G (Duncan & Thompson 1992; Thompson & Duncan 1995); this property alone is responsible for the different astrophysical signature of magnetars that sets them apart from other neutron stars. In observational parlance, magnetars manifest themselves as soft gamma-ray repeaters (SGRs) and anomalous X-ray pulsars, with high-energy emission in the X- and gamma-ray wavelengths (see Woods & Thompson 2004 for a review).

Of the two classes, SGRs are the more prolific objects in terms of high-energy outbursts. The bursts come in many shapes and forms, but the most spectacular events are the so-called *giant flares*. These release an enormous amount of energy ($\sim 10^{44}$ – 10^{46} erg), several orders of magnitude higher than the quiescence SGR luminosity. The only energy reservoir capable of fuelling such costly energy output is the ultra-strong magnetic field (Thompson & Duncan 1995, 2001).

Only three such giant flares have been observed to date, all in different objects: SGR 0526–66 (1979 March), SGR 1900+14 (1998 August) and SGR 1806–20 (2004 December). A major discovery that came with these events is the detection of quasi-periodic oscillations (QPOs) in the signal (Barat et al. 1983; Israel et al. 2005; Strohmayer & Watts 2005, 2006; Watts & Strohmayer 2006; Hambaryan, Neuhäuser & Kokkotas 2011). Since then, these observations have triggered a frenzy among neutron star theorists because they are taken as strong evidence for excited neutron star oscillations – indeed, the first evidence of this kind (an alternative interpretation of the QPOs could be based on magnetospheric physics, but this has attracted much less attention so far).

The early days of the ‘magnetar asteroseismology’ project were an attempt to explain the observed QPOs as elastic (seismic) modes excited in the neutron star crust (Duncan 1998; Messios, Papadopoulos & Stergioulas 2001; Piro 2005; Samuelsson & Andersson 2007). This scenario was a very attractive one because (i) giant flares are envisaged as the manifestation of a magnetic field instability that in the process fractures the crust and (ii) the low-frequency spectrum (\sim tens of Hz) of the axial-parity crustal modes is compatible with the presence of several $\lesssim 100$ Hz QPOs. However, it was soon realized that the real system is likely to display a much more complex behaviour because of the strong magnetic coupling between the crust and the core (Glampedakis, Samuelsson & Andersson 2006; Levin 2006).

★ E-mail: d.i.jones@soton.ac.uk

In effect, this coupling leads to global magnetic oscillations in which both the core and the crust may participate. To make things worse, the type of oscillations most relevant to magnetar QPOs (axisymmetric and axial Alfvén modes) could exist in the form of a *continuum* of frequencies, rather than a set of discrete frequencies (Levin 2007; Sotani et al. 2008; van Hoven & Levin 2008; Cerdá-Durán, Stergioulas & Font 2009; Colaiuda, Beyer & Kokkotas 2009; Colaiuda & Kokkotas 2011; Gabler et al. 2011, 2012).

This Alfvén continuum is now known to be very efficient in redistributing the energy of an initially excited crust mode via resonant absorption (Levin 2007; van Hoven & Levin 2008; Gabler et al. 2011, 2012). On the other hand, for oscillations of different symmetry (non-axisymmetric, polar, coupled axial-polar modes), the frequency spectrum may be discrete (e.g. Sotani et al. 2008; Lander & Jones 2011; Colaiuda & Kokkotas 2012).

The participation of the stellar core in the models of QPOs has highlighted the need for a better understanding of more exotic properties, such as the presence of superfluid and superconducting matter. These have an important impact on the mode spectrum and should be part of any ‘realistic’ magnetar model (Andersson, Glampedakis & Samuelsson 2009b; Gabler et al. 2013; Passamonti & Lander 2013).

In the recent years significant progress has been achieved with models that include crust–core coupling, superfluidity and axial-polar mode couplings (see references above). Although these models can in principle ‘explain’ many of the QPOs (albeit with some fine tuning), the truth is that the modern version of magnetar asteroseismology is plagued with a high degree of degeneracy because of the many degrees of freedom associated with the magnetic field and the superfluid state of matter.

At the same time, all the effort put in this problem so far has to do with making predictions about the mode frequencies. However, the actual QPOs offer more potential ‘observables’ than just the frequencies: for instance, their individual amplitudes and life spans will reflect properties of the flare and the stellar oscillations themselves.

This paper adds one more level of complexity to the problem by considering two important physical mechanisms related to the superfluid/superconducting nature of the stellar interior, which have received little attention thus far. Both are made possible by the rather large amplitude of the oscillations that are expected to be excited by the magnetar flare events. One concerns the potential destruction of superfluidity when the oscillation amplitude is sufficiently large, an effect considered recently by Gusakov & Kantor (2013). This effect will influence both oscillation decay time-scales and (by determining the fraction of the stellar inertia that participates in the oscillation) the frequencies. The other concerns the interaction between the rotation vortices in the neutron fluid and the magnetic flux tubes in the proton superconducting fluid. As has been studied recently (Haskell, Glampedakis & Andersson 2013), a sufficiently large oscillation can cause one to cut through the other, adding a strong source of dissipation to the oscillation.

Depending upon the initial amplitude of the excitation, we will argue that an excited mode could evolve by following three distinct ‘pathways’, characterized by different frequency evolutions and damping time-scales. Based on these evolutionary scenarios, we will argue that extra care must be taken when one attempts to theoretically identify the observed QPO frequencies and do ‘asteroseismology’ (i.e. infer the stellar equation of state, the magnetic field intensity and geometry). We also demonstrate the potential importance of the launching of magnetic waves into the magnetosphere as a possible damping mechanism for these oscillations.

Note for the ‘fast-track’ reader: the paper is structured in a way that allows the independent study of the ‘physics’ sections (results and conclusions – Sections 2 and 5) without the need of being exposed to any of the technical details on magnetar oscillations (these are discussed in Sections 3 and 4).

2 EVOLUTIONARY SCENARIOS FOR THE QPOS

2.1 Key magnetic field thresholds

A prerequisite for formulating ‘evolutionary paths’ for magnetar oscillations excited during a flare event is to understand how the induced magnetic field perturbation δB measures up against two key magnetic field thresholds. One threshold concerns the breaking of superfluidity, while the other concerns the breaking of the pinning between the magnetic flux tubes and the neutron vortices. We will now estimate the magnetic field perturbation induced by a flare, as well as these two thresholds. Note that some technical details are drawn from the following sections.

A magnetar flare is envisaged as a violent event triggered by the cracking of the neutron star crust as a result of magnetic field activity (Thompson & Duncan 1995, 2001). This will excite the star’s normal modes, which can be idealized as falling into two classes, *crustal* modes, confined mainly to the crust, and *Alfvén* modes, of a more global character, with predominantly elastic and magnetic restoring forces, respectively.

According to this model, prior to the fracture the evolving magnetic field exerts a growing strain on the crust; the crust responds elastically and the resulting quasi-static balance between the magnetic and elastic forces, F_{mag} and F_{el} , respectively, takes the form (see Section 3 for more details)

$$F_{\text{mag}} \approx F_{\text{el}} \Rightarrow \frac{B\delta B}{4\pi} \approx \mu\psi, \quad (1)$$

where ψ is the dimensionless strain and μ is the crust’s shear modulus. Instead of using the shear modulus itself (which is a rapidly varying parameter across the crust), it is much more convenient to work with the shear speed

$$v_s^2 = \frac{\mu}{\rho}, \quad (2)$$

where ρ is the total density. This quantity has a clear physical meaning (it represents the speed of elastic waves) and remains almost uniform throughout the crust (see for instance fig. 1 of Glampedakis & Andersson 2006).

At the moment of the fracture, ψ attains the value ψ_{br} and we can obtain a corresponding δB_{br} :

$$\frac{\delta B_{\text{br}}}{B} \approx \psi_{\text{br}} \frac{v_s^2}{v_A^2} \Rightarrow \frac{\delta B_{\text{br}}}{B} \approx \left(\frac{\psi_{\text{br}}}{0.1} \right) \frac{\rho_{14} v_{s,8}^2}{B_{15}^2}, \quad (3)$$

where v_A is the Alfvén speed for waves in normal (i.e. non-superconducting matter), defined by

$$v_A^2 = \frac{B^2}{4\pi\rho}. \quad (4)$$

and $v_{s,8} = v_s/10^8 \text{ cm s}^{-1}$. To produce the second equation, we have used the scalings $B_{15} = B/10^{15} \text{ G}$, $\rho_{14} = \rho/10^{14} \text{ g cm}^{-3}$. In addition, the breaking strain ψ_{br} has been normalized to the value suggested by the state-of-the-art simulations of Horowitz & Kadau (2009). This sudden removal of strain will lead to an unbalanced magnetic

stress, so we can expect the excitation of magnetic field oscillations at a level $B(0)$ at around this level:

$$\delta B(0) \lesssim \delta B_{\text{br}}. \quad (5)$$

The perturbation would then decay in time, according to the various mechanisms considered later in this paper.

The time-evolving magnetic perturbation $\delta B(t)$ is to be compared with the threshold, δB_{pin} , which makes contact with the likely presence of superfluid and superconducting matter in the outer neutron star core. In that region of the star neutron, vortices are expected to be pinned on to the much denser array of proton flux tubes (Sauls 1989). The magnetars, being slowly spinning and highly magnetized objects, are favoured for harbouring long-term pinned vortices (Glampedakis & Andersson 2011). A generic core oscillation excited during a flare will be associated with a non-vanishing velocity difference w between the neutron and proton fluids (see Section 3 for details). As a result of this velocity difference, there will be a Magnus force acting on a unit length segment of any individual pinned vortex, doing work against the pinning force exerted on the same segment by the flux tubes. Pinning cannot be sustained once w exceeds a critical lag w_{pin} (see Link 2003 and Section 4.4 for the detailed form of this quantity).

For a global magnetar mode, the magnetic field provides the main restoring force; in that case we can use equation (24) (see Section 3) which is a simple approximate relation between w and δB for global Alfvén-type oscillations. We can then obtain the threshold δB_{pin} required for vortex unpinning:

$$w = w_{\text{pin}} \Rightarrow \frac{\delta B_{\text{pin}}}{B} \sim \frac{w_{\text{pin}}}{v_A} \approx 4 \times 10^{-3}, \quad (6)$$

where now v_A is the Alfvén speed appropriate for a wave propagating in the superconducting proton fluid (of density $\rho_p = x_p \rho$, where x_p is the proton fraction):

$$v_A^2 = \frac{H_c B}{4\pi \rho_p} \quad (7)$$

and we have used typical values $\rho_{14} = 1$, $x_p = 0.05$ and $H_c = 10^{15}$ G for the density, the proton fraction and the (lower) critical superconductivity field, respectively.

The second magnetic field threshold, δB_{SF} , is related to the possibility of locally suppressing neutron superfluidity. This can be achieved once the relative motion between the superfluid and the normal components exceeds the so-called Landau critical speed. The destruction of superfluidity has been only recently discussed in the context of neutron stars by Gusakov & Kantor (2013) and our own analysis here makes use of their results.

As is described in detail in Section 3.1, the relation between w and δB is different for oscillations in the crust and in the core (see equations 24 and 29 below) and so we obtain *two* such thresholds. The detailed derivation is carried out in Section 3.2. For global Alfvén modes in the core, we obtain

$$\frac{\delta B_{\text{SF}}}{B} \sim 0.08 w_{\text{SF},7} B_{15}^{-1/2}, \quad (8)$$

where $w_{\text{SF},7} = w_{\text{SF}}/10^7 \text{ cm s}^{-1}$ is the normalized critical speed for the destruction of superfluidity. For elastic modes confined in the crust, we similarly have

$$\frac{\delta B_{\text{SF}}}{B} \sim \left(\frac{m_n^*/m_n}{15} \right) \frac{w_{\text{SF},7}}{v_{s,8}}, \quad (9)$$

where m_n^* is the effective mass of the entrained superfluid neutrons in the crust.

We observe that according to the above formulae, we should expect to have

$$\delta B_{\text{pin}} < \delta B_{\text{SF}}. \quad (10)$$

As we are about to see in the discussion below, the thresholds δB_{pin} and δB_{SF} for the perturbed magnetic field play a key role in understanding the time evolution of magnetar oscillations and making predictions about their observational signature.

That such large perturbations as these might be excited by a flare follows naturally from the Thompson & Duncan magnetar model, coupled with the very large breaking strains for (certain parts of) the neutron star crust computed using large molecular dynamics simulations (Horowitz & Kadau 2009). The sudden release of a breaking strain $\psi_{\text{br}} \sim 0.1$ will induce non-radial crustal motion on length-scales of the order of $\psi_{\text{br}} R \sim 1$ km. From the magnetic induction equation (see equation 14 below), this would correspond to a magnetic field perturbation $\delta B/B \sim 0.1$, of the high level required to break the superfluidity, as given by equation (8) above. The corresponding crustal displacement for breaking the pinning is about two orders of magnitude smaller (see equation 6 above), with amplitude ~ 10 m. Observations themselves show very high levels of fractional modulation of the electromagnetic output, at around the 20 per cent level. As noted by D’Angelo & Watts (2012), it is in fact difficult to account for such high levels of modulation, even when beaming of the emission is invoked. A large mode amplitude tends to reduce this problem, and is certainly consistent with (although not necessarily implied by) the observations.

2.2 The three evolutionary pathways

There are three key magnetic quantities that are of importance for magnetar flares. These are (i) $\delta B(0)$, the initial value of the magnetic field perturbation, which we expect to be bounded by $\delta B(0) \lesssim \delta B_{\text{br}}$; (ii) δB_{SF} , the critical perturbation above which superfluidity is destroyed; (iii) δB_{pin} , the critical perturbation above which pinning between vortices and flux tubes is broken, so that the dissipative process of flux tube cutting occurs. As given above, we expect $\delta B_{\text{pin}} < \delta B_{\text{SF}}$, so that there are *three* possible orderings of the three quantities, depending upon the value of $\delta B(0)$ relative to the other two. The magnetic field perturbation itself, $\delta B(t)$, will decay in time, generating three distinct evolutionary pathways, illustrated in the flowchart of Fig. 1, which we will describe below.

Before doing so, we will mention another important part of this story – the damping of the modes. We consider damping in detail in Section 4. There are two main sorts. Modes can be damped by either *external* or *internal* mechanisms. The external damping involves the launching of Alfvén waves into the magnetosphere, whose energy is eventually converted into an outward particle flux. This acts on both Alfvén and crustal modes. The efficiency of this process depends upon the fraction of the stellar surface which launches such waves. We consider three possibilities: emission from the entire stellar surface, emission only from a polar cap defined by the velocity-of-light cylinder and emission only from a polar cap defined by an ‘Alfvén radius’. The last of these seems to dominate, so is probably the most relevant. The internal damping includes mutual friction, which can be due to the cutting of magnetic flux tubes by neutron vortices as described above, or the more conventional scattering of electrons off neutron vortices. This applies only to the Alfvén modes, as this mechanism requires relative motion between the interior neutron vortices and the charged component of the star. A summary of our order-of-magnitude estimates of these various

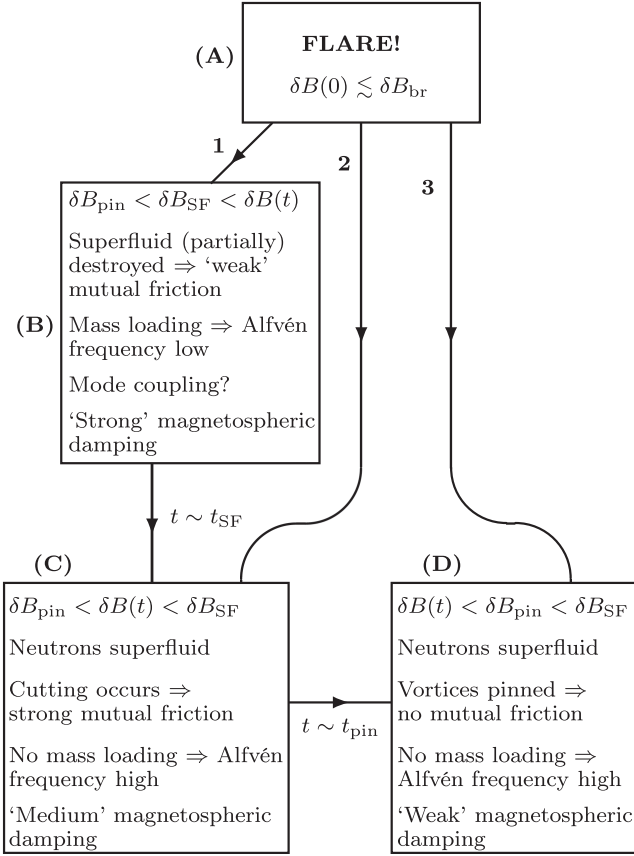


Figure 1. Flowchart illustrating the three evolutionary scenarios (1, 2, 3). The various boxes (A, B, C, D) describe different stages of evolution, with all scenarios beginning in box A, which represents the onset of the flare itself. The boxes give the range of magnetic field perturbations $\delta B(t)$ to which they apply, the predominant nature of the neutron fluid (normal/superfluid), information on the interaction between the vortices and flux tubes (pinning/cutting), information on 'mass loading' (i.e. whether the full stellar inertia participates in the Alfvén oscillation or just some fraction) and a comment on the likely damping mechanisms that apply.

time-scales is given in Table 1. Derivations of all of these results is given in Section 4.

Having set the scene, we can now describe the three distinct evolutionary pathways, illustrated in the flowchart of Fig. 1. We begin by considering only Alfvén modes. As will be explained below, the story for crustal modes is much simpler. All pathways start in box A, which simply represents the cracking event itself, at time $t = 0$.

In pathway 1, we have, at early times, $\delta B_{\text{pin}} < \delta B_{\text{SF}} < \delta B(t)$. In this case, the initial perturbation of the star is large enough to destroy the superfluidity, as represented by box B. This means that the neutrons and protons are tightly coupled, so that the Alfvén modes are 'mass loaded', i.e. the full stellar inertia plays a role in determining the mode frequencies. The Alfvén speed is then given by

$$v_A^2 = \frac{H_c B}{4\pi\rho}, \quad (11)$$

with the corresponding mode frequencies being $\omega \sim v_A/L$, where L is the mode's wavelength (typically this would be comparable to the stellar radius R). The tight coupling of neutrons to the charged component eliminates mutual friction as a damping mechanism, so in this case external damping is likely to dominate, probably with

a time-scale given by the 'Alfvén radius' column of Table 1 (i.e. equation 60). We should also note that the large mode amplitudes of this regime may mean that mode-mode coupling is important also, but we have no estimate of this.

After a time $\sim t_{\text{SF}}$, of the order of the magnetospheric decay time of equation (60), the perturbation has decayed to the point such that $\delta B(t)$ is no longer large enough to destroy the superfluidity at any point in the star. We then have $\delta B_{\text{pin}} < \delta B(t) < \delta B_{\text{SF}}$, as represented by box C. The superfluid nature of the neutrons suppresses any microscopic coupling between them and the protons, such that the Alfvén modes are no longer mass loaded, i.e. only the inertia of the charged component plays a role in determining the mode frequency, and the Alfvén speed is given by equation (7), which amounts to making the replacement $\rho \rightarrow \rho_p$ in equation (11). Simultaneously, cutting occurs between the magnetic flux tubes and the (newly formed) neutron vortices, opening up mutual friction, a new and powerful mechanism for damping, probably dominated by the cutting itself, rather than the scattering of electrons off the flux tubes, as indicated by the last two columns of the table. We can therefore expect the frequencies of Alfvén modes to *increase* at $t \sim t_{\text{SF}}$, by a factor of $\sim (\rho/\rho_p)^{1/2} \approx x_p^{-1/2} \approx 4$, while their damping time *decreases* to a value given by equation (96), which is itself a function of $\delta B(t)$.

After a time t_{pin} , of the order of the flux tube cutting time-scale of equation (96), the perturbation will decay to the point where $\delta B(t) < \delta B_{\text{pin}} < \delta B_{\text{SF}}$, as represented by box D. Now the pinning has been re-established. This will not have any effect on mode frequencies, but will shut off the powerful damping mechanism of flux tube cutting, so that the decay time of the Alfvén modes will increase, reverting again to a value determined by the launching of Alfvén waves into the magnetosphere, as per equation (60).

It is important to note that the transitions in damping and mass loading between the different regimes will not be perfectly sharp.¹ This is because the mode eigenfunctions for the axisymmetric ($m = 0$) modes thought to be relevant to magnetar flares vanish at the origin, so there will always be a small volume around the origin where the velocity is less than any given critical value. Also, such modes have a time dependence proportional to $\sin \omega t$, so that there will be oscillation phases where the velocity perturbation of *all* points in the star vanishes, so the velocity is again less than any given critical value. This means that a star in our regime B will contain points at which the strong mutual friction/non-mass-loaded conditions of regime C apply, while there will be points for a star in our regime C where the weak mutual friction conditions of regime D apply. For stars where the perturbation $\delta B(t)$ is much greater than the relevant threshold (δB_{SF} or δB_{pin}), these volumes/times will be short compared to the total stellar volume/oscillation period, but will have the effect of smoothing the transitions between the different regimes when the perturbation $\delta B(t)$ exceeds the critical value by only a small amount.

Intuitively, given the strong damping that applies in box C, we might expect there to be some significant mutual friction damping even in the regime of box B, due to superfluid at locations/times where the perturbation is small, giving a relatively smooth transition from B to C. Similarly, we might expect there to be a rather abrupt decrease in the damping rate in the transition C to D, with the weak damping of D applying only when there are no times/locations where the velocity exceeds the critical value.

To confirm this intuition concerning damping rates, we have carried out some investigations of these effects using simple

¹ We are grateful to the anonymous referee for alerting us to this issue.

Table 1. Table of *approximate* damping times, for both crustal and Alfvén modes. All times in seconds, and relevant equation numbers are given. The first column labels the type of mode. The second, third and fourth columns give the damping times for magnetospheric damping, assuming emission over the full surface, over a polar cap defined by the velocity-of-light cylinder and over a polar cap defined by the Alfvén radius, respectively. The fifth and six columns give the damping times for mutual friction, assuming flux tube cutting and electron scattering, respectively, relevant for Alfvén modes only.

Damping mechanism:	Magnetospheric damping			Mutual friction	
	Full surface	Velocity-of-light cylinder	Alfvén radius	Flux tube cutting	Electron scattering
Crustal mode	30 (eqn. 66)	10^6 (eqn. 67)	$30(\delta B/B)^{-2/3}$ (eqn. 68)	N/A	N/A
Alfvén mode	4 (eqn. 56)	10^{10} (eqn. 58)	$4(\delta B/B)^{-4/3}$ (eqn. 60)	$3(\delta B/\delta B_{\text{pin}})^{3/2}$ (eqn. 96)	10^3 (eqn. 101)

oscillator toy models. We considered the transverse vibrations of a one-dimensional string with velocity $v(x, t)$, parametrized by a maximum amplitude v_0 , acted upon by a drag force proportional to $-\lambda_{>}v$ for $|v(x, t)| > v_c$ and proportional to $-\lambda_{<}v$ for $|v(x, t)| < v_c$. In the case where $\lambda_{>}/\lambda_{<} \gg 1$, as describes the transition C \rightarrow D above, we do indeed find that the transition is sharp, in the sense that even when the mode amplitude has fallen to just twice the critical value (i.e. $v_0 = 2v_c$), the damping rate is 85 per cent of the rate calculated assuming $\lambda = \lambda_{>}$ always. In the case where $\lambda_{>}/\lambda_{<} \ll 1$, as describes the transition B \rightarrow C above, we find a more gradual transition. Setting $\lambda_{>}/\lambda_{<} = 0.1$, we find that when the velocity is within a factor of 2 of the critical value (again $v_0 = 2v_c$), the damping rate is 17 per cent of the value it would have if $\lambda = \lambda_{>}$ at all times.

Given the strong nature of the damping due to flux tube cutting, this level of damping should not be neglected in box B, which is why we use the term ‘weak mutual friction’ there. Extrapolating the results of the toy model we can quantify the strength of mutual friction in box B. The flux tube cutting time-scale entry in Table 1 (which represents the mutual friction time-scale in regime C) should be multiplied by a factor 10–100 for $\delta B \approx (1.5 - 5)\delta B_{\text{SF}}$, respectively.

We have also carried out some numerical experiments to gain more insight into the transition in mass loading, using a simpler toy model of a point oscillator (rather than a string), with mass $m = m_{>}$ for $|v(t)| > v_c$ and mass $m = m_{<}$ for $|v(t)| < v_c$. This represents the transition from the (mainly) mass-loaded state of regime B to the non-mass-loaded regime C. We chose the mass ratio $m_{<}/m_{>} = x_p$, equal to the proton mass fraction in the core, as is appropriate for such a transition. The mode period was calculated as a function of the ratio of the mode amplitude v_0 to the critical velocity, (v_0/v_c) . As was obviously to be expected, the mode frequency was found to increase by a factor $x_p^{-1/2}$ as the system transitioned from the $v_0/v_c \gg 1$ regime to the $v_0/v_c < 1$ regime.

Less obviously, we found a rather sharp transition from the higher frequency oscillation to the lower frequency one, occurring when v_0 was only slightly greater than v_c . For example, for $v_0 \approx 1.4v_c$, the time spent in the $m_{<}$ state is a meagre ≈ 0.08 fraction of the total oscillation period. We take this as evidence that the corresponding transition in a real star might be sharp and that the system in our box B is essentially mass loaded.

We can now move on to the second of our evolutionary pathways. In pathway 2, the initial value of the perturbation is assumed to be smaller than that for pathway 1, such that at early times $\delta B_{\text{pin}} < \delta B(t) < \delta B_{\text{SF}}$, so that box C applies. In this case, the neutrons are superfluid from the outset, but at early times the perturbation is large enough to break the pinning, so that the powerful damping mechanism of flux tube cutting is active. This will shut off after a time $\sim t_{\text{pin}}$ (of the order of the time-scale of equation 96), when pinning is restored and the Alfvén mode decay time will lengthen

to a value probably determined by the launching of Alfvén waves into the magnetosphere (equation 60), as represented by box D.

In pathway 3, the initial value of the perturbation is assumed to be small, such that $\delta B(t) < \delta B_{\text{pin}} < \delta B_{\text{SF}}$ initially, and therefore for all later times also, so that box D applies at all times. In this case, the neutrons are superfluid from the outset, and the vortices pinned to the flux tubes, so there is no evolution in Alfvén mode frequencies or damping times; the modes are never mass loaded, and the damping is always dominated by the launching of waves into the magnetosphere, as per equation (60).

The story for crustal modes is much simpler. If $\delta B(t)$ is greater than δB_{SF} , the crustal superfluidity will be destroyed. The strong coupling between the neutron and protons (i.e. the crustal lattice) then ensures that the crustal modes are fully mass loaded, so that $\omega \sim v_s/L$, with the full (crustal) mass density appearing in the expression for v_s (as in equation 2 above). However, the situation is very similar in the case $\delta B(t) < \delta B_{\text{SF}}$. In this regime, the neutrons are superfluid, but the strong entrainment believed to apply to the crustal superfluid effectively couples the neutrons to the protons, so the dynamics remains essentially unchanged. Meanwhile, the notion of a critical δB_{pin} does not apply for the crust, as the magnetic flux tubes open out into ‘classical’ (i.e. non-superconducting) flux bundles in the crust, so there is no notion of flux tube–vortex cutting. So, the crustal modes are, to a good approximation, unaffected by the transitions between the states B, C and D of the flow diagram that play such an important role for the Alfvén modes. For purely crustal modes, mutual friction is ineffective (because the crust segment of each vortex is not magnetized), so that the damping time-scale is likely to be dominated by the launching of Alfvén waves into the magnetosphere, as per equation (68).

In summary, for Alfvén modes, we have a rather rich set of possibilities. Pathway 1 is represented by A \rightarrow B \rightarrow C \rightarrow D in the flowchart, with changes occurring in both mode frequencies and damping times as the evolution proceeds. Pathway 2 has the flow A \rightarrow C \rightarrow D, with no frequency changes, but a change in damping time-scale. Pathway 3 is the simplest, represented by A \rightarrow D, with no sudden changes in any mode properties. For crustal modes, there are no corresponding transitions in mode properties.

In Sections 3 and 4, we provide detailed calculations to estimate the various damping time-scales that feature in the argument sketched above, leaving our concluding discussion of these ideas to Section 5.

3 THE DYNAMICS OF SUPERFLUID MAGNETARS

3.1 Multifluid formalism

The magnetohydrodynamics of magnetars can be formulated on the basis of a multifluid model for the stellar interior. Mature

magnetars older than 500 years or so are expected to be cold enough (Ho, Glampedakis & Andersson 2012) as to primarily consist of superfluid neutrons, superconducting protons and electrons (the possibility of having exotic types of matter in the inner core is not considered here). An additional component is the solid lattice in the crust which can be modelled as a positively charged elastic fluid. The equations of motion for this system are well known, see for example Andersson et al. (2009b).

There are two Euler equations, one for the neutrons and one for the ‘protons’, the latter component is identified either with the actual protons in the core or with the crustal lattice (plus the electrons in both regions).

In this paper, we are exclusively interested in fluid motion (to be more precise, oscillations) which is accompanied by negligible perturbations in the fluid density and pressure with respect to their background values. This category of oscillations includes the modes that are typically invoked as the most likely interpretation behind the QPOs seen in magnetar flares (i.e. axisymmetric axial-parity modes and non-axisymmetric polar-parity modes, both of which are nearly incompressible).

For this kind of motion, the linearized Euler equations in the stellar rotating frame take the form:

$$\partial_t(\mathbf{v}_n + \varepsilon_n \mathbf{w}) + 2\boldsymbol{\Omega} \times \mathbf{v}_n = \frac{1}{\rho_n} (\mathbf{F}_{mf} + \mathbf{F}_n) \quad (12)$$

$$\partial_t(\mathbf{v}_p - \varepsilon_p \mathbf{w}) + 2\boldsymbol{\Omega} \times \mathbf{v}_p = \frac{1}{\rho_p} (\mathbf{F}_{mag} + \mathbf{F}_{el} - \mathbf{F}_{mf} + \mathbf{F}_{visc}), \quad (13)$$

where \mathbf{v}_x ($x = n, p$) is the fluid velocity with respect to the background rigid body rotation with angular frequency $\boldsymbol{\Omega} = \Omega \hat{z}$ (we ignore any small spin lag that could be present between the various components), $\mathbf{w} = \mathbf{v}_p - \mathbf{v}_n$ is the proton–neutron velocity difference and ρ_x is the individual fluid density. The coupling due to the entrainment effect is encoded in the parameters ε_x . These are related to the effective particle masses m_x^* as $\varepsilon_x = 1 - m_x^*/m_x$ (Prix 2004).

The proton fluid in the core experiences a magnetic force \mathbf{F}_{mag} which represents the macroscopically averaged tension of the quantized flux tubes. A magnetic force \mathbf{F}_n is also exerted on the neutron superfluid in the core, as a result of the contribution of the entrained neutrons to the flux tube tension (see Glampedakis, Andersson & Samuelsson 2011 for details). In the region of the crust, \mathbf{F}_{mag} is replaced by the usual Lorentz force and \mathbf{F}_{el} is the elastic force exerted on the crustal lattice. The neutron–proton fluids are coupled through the mutual friction force \mathbf{F}_{mf} ; this represents any coupling between the fluids mediated through the neutron vortices. Finally, the proton fluid experiences a frictional force \mathbf{F}_{visc} arising from shear and bulk viscosity.

The additional dynamical equations are the continuity equations which for incompressible flow (as assumed here) take the form $\nabla \cdot \mathbf{v}_x = 0$, and the magnetic induction equation

$$\partial_t \delta \mathbf{B} = \nabla \times (\mathbf{v}_p \times \mathbf{B}), \quad (14)$$

where $\delta \mathbf{B}$ is the perturbed magnetic field.

We can re-write the pair of the Euler equations in an equivalent form in terms of the velocity difference \mathbf{w} and the average velocity $\mathbf{v} = x_p \mathbf{v}_p + (1 - x_p) \mathbf{v}_n$, where $\rho = \rho_n + \rho_p$ is the total density and $x_p = \rho_p / \rho$ is the ‘proton’ fraction.

The resulting ‘average’ and ‘difference’ Euler equations are, respectively,

$$\partial_t \mathbf{v} + 2\boldsymbol{\Omega} \times \mathbf{v} = \frac{1}{\rho} (\mathbf{F}_{mag} + \mathbf{F}_n + \mathbf{F}_{el}) \quad (15)$$

and

$$(1 - \bar{\varepsilon}) \partial_t \mathbf{w} + 2\boldsymbol{\Omega} \times \mathbf{w} = \frac{1}{\rho_p} (\mathbf{F}_{mag} + \mathbf{F}_{el} + \mathbf{F}_{visc}) - \frac{1}{\rho_n} \mathbf{F}_n - \frac{1}{x_p \rho_n} \mathbf{F}_{mf}, \quad (16)$$

where we have defined $\bar{\varepsilon} = \varepsilon_n + \varepsilon_p$ and used the property $\rho_n \varepsilon_n = \rho_p \varepsilon_p$ (Prix 2004).

In this work, we consider two idealized types of oscillations: (i) ‘Alfvén’ modes, where the restoring force is predominantly magnetic, and which involve fluid motion in the bulk of the core; (ii) ‘crustal’, where the restoring force is predominantly elastic, and which are confined mainly in the crust. Real magnetar oscillations may be some sort of hybrid, with properties intermediate between these two extremes.

Our analysis will require mode solutions at a level of the order of magnitude precision. For the modes we consider, the continuity equations are trivially satisfied and we can safely ignore the Coriolis force term because mature magnetars are slow rotators. The magnetic force can be approximated as (see Mendell 1991; Glampedakis et al. 2011 for the exact expression for this force)

$$\mathbf{F}_{mag} \sim \frac{H_c \delta B}{4\pi L}, \quad (17)$$

where L is the mode’s characteristic length-scale and $H_c \approx 10^{15}$ G is the (lower) critical field for superconductivity (Tilley & Tilley 1990). If \mathbf{F}_{mag} is taken to be the magnetic force in the crust (or, more generally, the magnetic force in the absence of superconductivity), we can still use (17) after making the replacement $H_c \rightarrow B$. From the general expression for \mathbf{F}_n (Glampedakis et al. 2011), we can also deduce that this force is smaller than \mathbf{F}_{mag} ,

$$\frac{F_n}{F_{mag}} \sim x_p \frac{\rho}{m_p^*} \frac{\partial m_p^*}{\partial \rho} \ll 1, \quad (18)$$

where m_p^* is the effective mass of the entrained protons. This is a slowly varying function of density, see for example Chamel (2008). Moreover, a plane-wave analysis as in Andersson et al. (2009b) reveals that \mathbf{F}_n does not lead to any modification to the propagation speed of Alfvén waves (see equation 7).

For the elastic force, we have

$$\mathbf{F}_{el} = \mu \nabla^2 \xi_p \rightarrow F_{el} \sim \rho v_s^2 \frac{\xi_p}{L^2}, \quad (19)$$

where μ is the crustal shear modulus, $v_s^2 = \mu / \rho$ is the shear speed and ξ_p is the displacement of the crustal lattice (it is related to the strain in the crust as $\xi_p \sim \psi L$). The displacement vector can be eliminated with the help of the induction equation (14), i.e. $\xi_p \sim L \delta B / B$, leading to

$$F_{el} \sim \frac{\rho v_s^2 \delta B}{L B}. \quad (20)$$

The standard method for calculating modes of dissipative systems is to find a mode solution without initially including the frictional forces (in our case \mathbf{F}_{mf} and \mathbf{F}_{visc}). The dissipative action of these forces is subsequently accounted for by using the inviscid mode solution in suitable energy integral expressions. This will be our approach too in the calculation of the damping of magnetar oscillations (see Section 4).

The mode property most relevant for our analysis is the relative proton–neutron velocity \mathbf{w} . A simple inspection of the difference Euler equation (16) reveals that this countermoving degree of

freedom is a generic property of the modes considered here. From the same equation, we estimate

$$w \sim (1 - \bar{\varepsilon})^{-1} \frac{F_{\text{restore}}}{\omega x_p \rho}, \quad (21)$$

where ω is the mode's angular frequency and $F_{\text{restore}} = \{F_{\text{mag}}, F_{\text{el}}\}$ is the main restoring force.

Applying this formula to a global Alfvén mode (for which the entrainment prefactor is of order unity and $F_{\text{restore}} = F_{\text{mag}}$), we obtain

$$w \sim \frac{v_A^2}{L\omega} \frac{\delta B}{B}, \quad (22)$$

where we have used the Alfvén speed:

$$v_A^2 = \frac{H_c B}{4\pi\rho x_p}. \quad (23)$$

To the accuracy we are working, we can also approximate $v_A \sim \omega L$ to obtain

$$w \sim v_A \frac{\delta B}{B}. \quad (24)$$

Inserting the explicit form of v_A and parametrizing, we finally obtain

$$w \sim 10^8 \left(\frac{H_{15} B_{15}}{x_{5} \rho_{14}} \right)^{1/2} \frac{\delta B}{B} \text{ cm s}^{-1}, \quad (25)$$

where we have introduced the scalings $\rho_{14} = \rho/10^{14} \text{ g cm}^{-3}$, $H_{15} = H_c/10^{15} \text{ G}$, $x_5 = x_p/0.05$.

For crustal modes, $F_{\text{restore}} = F_{\text{el}}$ and we have

$$w \sim (1 - \bar{\varepsilon})^{-1} \frac{v_s^2}{L x_p \omega} \frac{\delta B}{B}. \quad (26)$$

In this case, we have retained the entrainment factor; detailed calculations suggest that the effective mass of the entrained superfluid neutrons could be much higher than the bare neutron mass, i.e. $m_n^* \gg m_n$ (Chamel 2005, 2012). We can then approximate (recall that $x_p \ll 1$ in the inner crust)

$$1 - \bar{\varepsilon} = 1 - \frac{\varepsilon_n}{x_p} \approx \frac{1}{x_p} \frac{m_n^*}{m_n}. \quad (27)$$

Then

$$w \sim \frac{m_n}{m_n^*} \frac{v_s^2}{L\omega} \frac{\delta B}{B}. \quad (28)$$

If we make the approximation $v_s \sim \omega L$, we finally obtain

$$w \sim \frac{m_n}{m_n^*} v_s \frac{\delta B}{B}. \quad (29)$$

Inserting numerical values

$$w \sim 7 \times 10^6 v_{s,8} \left(\frac{15}{m_n^*/m_n} \right) \frac{\delta B}{B} \text{ cm s}^{-1}, \quad (30)$$

where we have introduced the scaling $v_{s,8} = v_s/(10^8 \text{ cm s}^{-1})$ (recall that v_s stays almost uniform throughout the crust). The value of m_n^*/m_n in neutron star crusts is discussed in Andersson et al. (2009b); according to their fig. 1, which is in turn based on the calculations of Chamel (2005, 2012), a value of $m_n^*/m_n \approx 15$ is typical throughout much of the crust.

The above expressions for the velocity lag w will provide the key input for the calculations underpinning the evolutionary paths of Section 2.2.

Apart from these, we will also need an estimate for the mode's kinetic energy E_{mode} in order to compute damping time-scales in Section 4. For our two-fluid system, this energy receives contributions from both the comoving and counter-moving degrees of freedom (see for instance Andersson, Glampedakis & Haskell 2009a),

$$E_{\text{mode}} = \frac{1}{2} \int dV \rho \left[v^2 + x_p(1 - x_p) \left(1 - \frac{\varepsilon_n}{x_p} \right) w^2 \right]. \quad (31)$$

From the Euler equations, it also follows (after eliminating $\mathbf{F}_{\text{restore}}$) that

$$\mathbf{v} \approx x_p(1 - \bar{\varepsilon})\mathbf{w}. \quad (32)$$

An Alfvén-type mode would then represent a mainly counter-moving oscillation,

$$\mathbf{v} \approx x_p \frac{m_p^*}{m_p} \mathbf{w} \ll \mathbf{w}. \quad (33)$$

Note that a typical range for the entrained proton mass is $0.3 < m_p^*/m_p < 0.8$ (Chamel 2008). The mode energy (31) is dominated by the second, counter-moving, term. We can easily obtain

$$E_{\text{mode}} \approx \frac{1}{2} \int dV \rho x_p \frac{m_p^*}{m_p} w^2. \quad (34)$$

In the case of crustal modes, and as a result of the strong entrainment coupling, we find a dominantly comoving character:

$$\mathbf{v} \approx \frac{m_n^*}{m_n} \mathbf{w}. \quad (35)$$

This time the mode energy is dominated by the first term, and the energy formula becomes essentially that of a single-component system,

$$E_{\text{mode}} \approx \frac{1}{2} \int dV \rho v^2, \quad (36)$$

where, for a crustal mode, the integral should be taken over the region of the crust.

3.2 Destruction of superfluidity

In a recent publication, Gusakov & Kantor (2013) have argued that a sufficiently large velocity difference between the superfluid and non-superfluid components can destroy the superfluidity in neutron stars – a phenomenon also seen in laboratory systems. More accurately, the superfluid energy gap Δ is not only a function of temperature T , but is also a function of the relative velocity between the superfluid and the normal components. The gap is suppressed when this relative motion increases. In our case, the normal component is identified with the electrons which in turn are nearly comoving with the proton fluid. Therefore, the relevant relative velocity is \mathbf{w} and $\Delta = \Delta(T, w)$.

The main result of Gusakov & Kantor (2013) is their equation 12 which gives an expression for the critical relative velocity w_{SF} between the superfluid and normal components above which superfluidity is destroyed:

$$w_{\text{SF}} = 10^7 \left(\frac{\Delta(T, 0)}{10^9 \text{ K}} \right) \left(\frac{\rho_0}{\rho} \right)^{1/3} \text{ cm s}^{-1}, \quad (37)$$

where $\rho_0 = 0.16 \text{ fm}^{-3}$ is the nuclear density and the neutron pairing gap has been normalized to a canonical value.

Clearly, it is interesting to compare this velocity with the w defined above, which gives the superfluid–charged particle velocity difference for an Alfvén-type oscillation. Comparison with

equation (25) above shows that, for Alfvén modes, we can expect the actual velocity difference w to exceed the critical value for destroying the superfluidity for $\delta B/B \sim 0.1$, indicating that the larger flare events may well push the star over this critical threshold. Comparing instead with equation (30) above we see that, for crustal modes, somewhat larger perturbations in the magnetic field are required to break the superfluidity, with $\delta B/B \sim 1$. This is large, but, given the order-of-magnitude nature of our estimates, the possibility of crustal modes also breaking the superfluidity cannot be excluded.

As discussed in Section 2.1 above, for the purposes of describing the evolution of a magnetar flare, it is convenient to recast our results in terms of $\delta B/B$, the critical (fractional) perturbation in magnetic field above which superfluidity is destroyed. To do so, for Alfvén modes, we set $w = w_{\text{SF}}$ in equation (24) above and invert to give

$$\frac{\delta B_{\text{SF}}}{B} \sim \frac{w_{\text{SF}}}{v_A}. \quad (38)$$

Parametrizing:

$$\frac{\delta B_{\text{SF}}}{B} \sim 0.08 \left(\frac{x_5 \rho_{14}}{H_{15} B_{15}} \right)^{1/2} w_{\text{SF},7}, \quad (39)$$

where $w_{\text{SF},7} = w_{\text{SF}}/10^7 \text{ cm s}^{-1}$. For crustal modes, we similarly set $w = w_{\text{SF}}$ in equation (29) to give

$$\frac{\delta B_{\text{SF}}}{B} \sim \frac{m_n^* w_{\text{SF}}}{m_n v_A}. \quad (40)$$

Parametrizing:

$$\frac{\delta B_{\text{SF}}}{B} \sim \left(\frac{m_n^*/m_n}{15} \right) \frac{w_{\text{SF},7}}{v_{s,8}}. \quad (41)$$

4 DAMPING OF MAGNETAR OSCILLATIONS

4.1 Magnetospheric damping: formalism

A stellar oscillation that involves motion of the stellar surface will also ‘shake’ the magnetic field lines, launching Alfvén waves in the magnetosphere. These waves effectively remove energy from the oscillation and dissipate it as they propagate out across the magnetosphere. This process could be relevant for dissipating magnetar oscillations excited during flare events and it is the purpose of this section to assess its efficiency.

Following the analysis of Ho & Lai (2000), we consider a typical fluid displacement ξ_0 on the stellar surface; the induced Alfvén wave will travel a distance $\sim c/\omega$ in the magnetosphere in one oscillation period. The resulting wave amplitude will be $\delta B \sim B\omega\xi_0/c$ – this is much smaller than magnetic field perturbation $\sim \xi_0 B/L$ induced in the stellar interior (see equation 14).

The radiated power is given by the following Poynting flux surface integral

$$P_A \approx \frac{c}{8\pi} \int dS \frac{\omega^2}{c^2} |\hat{\mathbf{B}} \cdot \hat{\mathbf{r}}| |\xi_0 \times \mathbf{B}|^2, \quad (42)$$

where $\hat{\mathbf{B}}$ and $\hat{\mathbf{r}}$ are unit vectors along the magnetic field and the radial direction, respectively. This can be approximated as

$$P_A \sim 4\pi R^2 c \frac{(\delta B)^2}{8\pi} \sim \frac{1}{2c} (\omega \xi_0 B R)^2. \quad (43)$$

These formulae allow for emission over the entire stellar surface. However, this is not necessarily a good assumption. First, it only really makes sense to talk of Alfvén waves on field lines whose total length is significantly longer than the wavelength of the Alfvén

waves. Secondly, as discussed in Thompson & Blaes (1998), it is likely that this flux only represents an energy loss for those field lines which are *open*. The idea is that Alfvén waves on open field lines propagate out far from the star and at some point become non-linear and radiate their energy away as electromagnetic waves and/or particles. The upshot of this effect is to suppress the flux as calculated by an all-surface integral by a factor, so as to allow for energy loss only from the *polar cap*, i.e. from on a patch of angular radius θ_{cap} , centred on the magnetic axis, defined to be the surface region from which open field lines emanate. In the following calculations, we will make the small-angle approximation $\sin \theta_{\text{cap}} \approx \theta_{\text{cap}}$, although there are situations where the polar cap can occupy a significant fraction of the stellar surface. Given the order-of-magnitude accuracy of other parts of our calculation, such an approximation is acceptable.

It is useful to relate θ_{cap} to the (cylindrical) radius of the last closed field line. To do so, note that a dipolar magnetic field line is given by the polar relation $r(\theta)$:

$$\frac{\sin^2 \theta}{r(\theta)} = \frac{1}{r(\pi/2)}, \quad (44)$$

assuming a dipole axis along $\theta = 0$. Suppose the last closed field line cuts the equatorial $\theta = \pi/2$ plane at a radius R_c . Then this field line is defined by the equation

$$\frac{\sin^2 \theta}{r(\theta)} = \frac{1}{R_c}. \quad (45)$$

It follows that this field line cuts the stellar surface $r = R$ at $\theta = \theta_{\text{cap}}$ given by $\sin \theta_{\text{cap}} = \sqrt{R/R_c}$. We can therefore approximate

$$\theta_{\text{cap}} \approx \sqrt{\frac{R}{R_c}} \lesssim 1. \quad (46)$$

The precise value of R_c then depends upon which physical mechanism is responsible for determining the last closed field line. This argument will hold up to geometric factors of order unity for non-aligned dipoles, i.e. dipole whose symmetry axes do not lie along $\theta = 0$. Note that the polar cap will always be centred on the magnetic dipole axis, not the rotation axis.

It is standard practice in modelling neutron star magnetospheres (especially those of radio pulsars) to place the last open field line at the location (or thereabouts) where the rotational velocity of the field lines equals the speed of light, i.e. the location of the light cylinder $R_L = c/\Omega$ (e.g. Goldreich & Julian 1969). We then have, using equation (46),

$$\theta_L \approx \sqrt{\frac{2\pi R}{cP}} \approx 0.015 R_6^{1/2} \left(\frac{P}{1\text{ s}} \right)^{-1/2}. \quad (47)$$

In addition to the finite rotation of the system, there is another mechanism that can cause the lines to become open, active only in dynamically perturbed (rather than rigidly rotating) magnetospheres. This mechanism has been discussed by Thompson & Blaes (1998). Consider a ‘tube’ of Alfvén waves propagating out along the field lines that originate from the polar cap. The magnetic pressure from the (background) dipolar field scales as B^2 , which is a steeply decaying function of distance from the star ($\sim r^{-6}$). The Alfvén wave pressure is a less steep function [recall that $\delta B \sim B^{1/2}$ for the travelling Alfvén wave (Blaes et al. 1989)]. Thompson & Blaes (1998) argue that there then exists a critical ‘Alfvén radius’ at which the Alfvén stresses dominate the magnetic dipole ones, thus opening

up the field lines. Thompson & Blaes (1998) calculate a polar cap angular radius

$$\theta_A \approx \left(\frac{\delta B}{B} \right)^{1/3}, \quad (48)$$

where both B and δB are to be evaluated at the stellar surface. The dependence on δB makes this cap radius dependent upon the amplitude of the perturbation.

To gain some insight, we can easily calculate the ranges in polar cap radius corresponding to the various stages in evolution of Alfvén modes discussed in Section 2.2. For the evolutionary stage represented by box B in the flowchart of Fig. 1, we can combine equations (3), (8) and (48) to obtain

$$\delta B_{\text{SF}} < \delta B < \delta B_{\text{br}} \iff 0.4 \lesssim \theta_A \lesssim 1. \quad (49)$$

For the evolutionary stage represented by box C in the flowchart, we can also use equation (6) to obtain

$$\delta B_{\text{pin}} < \delta B < \delta B_{\text{SF}} \iff 0.16 \lesssim \theta_A \lesssim 0.4. \quad (50)$$

For crustal modes, the threshold δB_{pin} is irrelevant, while the value of δB_{SF} is given by equation (9), which, when combined with equation (48), gives a corresponding polar cap radius of order unity.

Comparing the above results with equation (47) above, we see that for both Alfvén and crustal modes, the polar cap radius in the present case can be much larger than the one in the light-cylinder model. More quantitatively, this opening of field lines due to Alfvén pressure will be the determining factor in fixing θ_{cap} when $\theta_A > \theta_L$. Combining equations (47) and (50), we see that this is the case when $P > 0.02R_6^{1/2}$ s. This is clearly well satisfied for magnetars.

There is another modification of the Poynting flux due to the open field lines that has to do with the nature of the oscillation mode itself. For most classes of modes, we would expect that the fluid displacement in the cap would be $\xi_{\text{cap}} \approx \xi_0$. However, for magnetic Alfvén modes, the mode eigenfunction will vanish on the magnetic axis, and we would expect $\xi_{\text{cap}} \approx \xi_0 \theta$ in the vicinity of the magnetic axis. We will therefore estimate the Alfvén flux as

$$P_A \approx \frac{R^2}{4c} \theta_{\text{cap}}^2 (\omega \xi_{\text{cap}} B)^2, \quad (51)$$

with

$$\xi_{\text{cap}} \approx \xi_0 \theta_{\text{cap}} \quad \text{for Alfvén modes,} \quad (52)$$

$$\xi_{\text{cap}} \approx \xi_0 \quad \text{for other modes.} \quad (53)$$

We will proceed by first evaluating the Poynting fluxes and magnetospheric damping times by performing a naive full-surface integral for crustal modes and Alfvén modes, making use of equation (43). The damping time-scale τ_A will be calculated with the help of the standard formula

$$\tau_A = \frac{E_{\text{mode}}}{P_A}, \quad (54)$$

where E_{mode} is the mode energy. We will then calculate damping times in the case where the location of the magnetospheric light cylinder defines the last closed field line, making use of equations (51) and (47). We will then repeat this procedure for the case where the Alfvén radius defines the last closed field line, again making use of equation (51), this time combined with equation (48). Of course, this is just a rough estimate; a more accurate calculation would solve for the integral in equation (42) over the appropriate range in θ , inserting the correct inclined-dipole geometry and mode eigenfunction. This, however, seems an overkill given that we

are looking for approximate indications of what are the important damping mechanisms for magnetar oscillations.

In the calculations that follow, we first present the damping assuming emission over the full surface, which we are then able to easily modify to allow for emission only over a polar cap, defined either by the last closed field line or balance between the magnetic and Alfvén pressures. It is these last two results that we consider to be the realistic ones, so it is the *shorter* of these two that we expect to be relevant in a magnetar. (This in fact proves to be the result obtained by balancing the magnetic and Alfvén pressures; compare columns 3 and 4 of Table 1.)

4.2 Magnetospheric damping: Alfvén modes

As we have already discussed, the Alfvén-type modes are assumed to be global oscillations, extending over the bulk of the neutron star core. The mode energy has been given in (34). For the purposes of the present calculation, we can approximate that expression by assuming that ξ_0 is comparable to the fluid displacements in the core, that is, $w \sim \omega \xi_0$. Then

$$E_{\text{mode}} \sim \frac{1}{2} x_p \rho \omega^2 \xi_0^2 V_*, \quad (55)$$

where V_* is the stellar volume.

Combining the mode energy with the Poynting flux (43) for the entire surface, we obtain the following estimate for the damping time-scale:²

$$\tau_A \sim \frac{x_p M c}{B^2 R^2} \sim 4 x_5 M_{1.4} R_6^{-2} B_{15}^{-2} \text{ s}, \quad (56)$$

where $M_{1.4} = M/1.4 M_\odot$.

We will now re-evaluate the Alfvén fluxes assuming energy losses only along open field lines, assuming that the last closed field line is defined by the velocity-of-light cylinder. Using equations (43) and (52) we obtain new, longer, damping times. The flux P_A now contains a factor of θ_L^4 :

$$P_A \sim \pi^2 \frac{R^4}{c^3 P^2} (\omega \xi_0 B)^2. \quad (57)$$

The mode energy is the same as before, and we thus obtain the (much longer) time-scale

$$\tau_A \sim \frac{x_p}{2\pi^2} \frac{M c^3 P^2}{R^4 B^2} \approx 10^{10} x_5 \left(\frac{P}{10 \text{ s}} \right)^2 \frac{M_{1.4}}{R_6^4 B_{15}^2} \text{ s}. \quad (58)$$

For the case where the polar cap radius is determined by the magnetic pressure, we can again use (43) and (52) with $\theta_{\text{cap}} = \theta_A$:

$$P_A \sim \left(\frac{\delta B}{B} \right)^{4/3} \frac{R^2}{4c} (\omega \xi_0 B)^2. \quad (59)$$

This time the damping time-scale is

$$\tau_A \sim \left(\frac{\delta B}{B} \right)^{-4/3} \frac{x_p M c}{B^2 R^2} \sim 4 \left(\frac{\delta B}{B} \right)^{-4/3} \frac{x_5 M_{1.4}}{B_{15}^2 R_6^2} \text{ s}. \quad (60)$$

Using the polar cap sizes of equations (49) and (50), we find that in the range $\delta B_{\text{SF}} < \delta B < \delta B_{\text{br}}$,

$$\tau_A \sim (0.05 - 150) x_5 M_{1.4} R_6^{-2} B_{15}^{-2} \text{ s}, \quad (61)$$

² We note that a more rigorous calculation for the damping of axial and axisymmetric Alfvén modes in a uniform density fluid sphere coupled with the Poynting flux (42) leads to a similar result.

and

$$\tau \sim (150 - 5 \times 10^3) x_5 M_{1.4} R_6^{-2} B_{15}^{-2} \text{ s}, \quad (62)$$

in the range $\delta B_{\text{pin}} < \delta B < \delta B_{\text{SF}}$. (Note that these time-scales, in common with some others that will follow below, depend upon the size of the perturbation itself. This non-exponential damping is characteristic of non-linear damping processes. Such time-scales are physically meaningful, having the interpretation of the time it takes for the mode to decay by a factor of order unity.)

As expected these time-scales lie somewhere between the full-surface and light-cylinder results, equations (56) and (58), respectively. It is also clear that the full-surface time-scale (56) and the (perhaps more realistic) polar cap-modified time-scale (61) are sufficiently short as to play a role in the evolutionary pathways discussed earlier in Section 2.2. On the other hand, the light-cylinder time-scale (58) is too long to have any bearing on our analysis.

4.3 Magnetospheric damping: crustal modes

The second class of oscillations under consideration is that of crustal elastic modes. For these modes, the fluid motion is confined inside the crust.

As before, we will compute the damping time-scale τ_A by first using the full-surface Poynting flux (43), making no effort to account for the polar cap suppression factor. The mode energy is given by equation (36) and we can approximate that by assuming that $v \sim \omega \xi_0$. Then

$$E_{\text{mode}} \approx \frac{1}{2} \rho (\omega \xi_0)^2 V_{\text{crust}}, \quad (63)$$

where V_{crust} is the volume of the crust.

We obtain

$$\tau_A \sim c \rho \frac{V_{\text{crust}}}{B^2 R^2} \approx 3c \frac{M \Delta}{B^2 R^3}, \quad (64)$$

where Δ is the thickness of the crust (we have also used $\rho \approx 3M/4\pi R^3$ for the density in the inner crust). Choosing a typical thickness $\Delta = 0.1R$, we find³

$$\tau_A \sim 0.3 \frac{Mc}{B^2 R^2}, \quad (65)$$

or equivalently

$$\tau_A \approx 26 M_{1.4} R_6^{-2} B_{15}^{-2} \text{ s}. \quad (66)$$

If the magnetospheric damping is limited to the open field lines, then we have the revised time-scale [through equation (43) and the light-cylinder correction factor θ_{L}^2]:

$$\tau_A \sim 0.05 \frac{Mc^2 P}{B^2 R^3} \approx 10^6 \left(\frac{P}{10 \text{ s}} \right) M_{1.4} R_6^{-3} B_{15}^{-2} \text{ s}. \quad (67)$$

Lastly, if the open line region is determined by the magnetic pressure, the time-scale is modified by a factor θ_{A}^2 :

$$\tau_A \sim 0.3 \left(\frac{\delta B}{B} \right)^{-2/3} \frac{Mc}{B^2 R^2} \sim 30 \left(\frac{\delta B}{B} \right)^{-2/3} \frac{M_{1.4}}{B_{15}^2 R_6^2} \text{ s}. \quad (68)$$

For the amplitude range $\delta B_{\text{SF}} < \delta B < \delta B_{\text{br}}$, we have

$$\tau_A \sim (26 - 160) M_{1.4} R_6^{-2} B_{15}^{-2} \text{ s}, \quad (69)$$

³ This result is of the same order of magnitude as the more rigorous time-scale calculated for axial and axisymmetric crustal modes of a uniform crust coupled with the flux (42).

while for the range $\delta B_{\text{pin}} < \delta B < \delta B_{\text{SF}}$,

$$\tau_A \sim (160 - 10^3) M_{1.4} R_6^{-2} B_{15}^{-2} \text{ s}. \quad (70)$$

Apart from the light-cylinder result, all other damping time-scales are rather short and are potentially relevant in the analysis of the evolution of crustal modes.

4.4 Internal damping: friction due to flux tube cutting

The co-existing and possibly intersecting neutron vortices and proton flux tubes in the outer core of neutron stars can lead to a substantial mutual friction force F_{mf} between the fluids. The basic reason behind the strong vortex–flux tube interaction is their intrinsic (mesoscopic) magnetic fields. The force at a single intersection site is given by the ratio of the local magnetic interaction energy E_{int} to the range of the magnetic forces, which can be taken to be the London penetration length Λ . That is, after ignoring geometric factors of order unity (Ruderman, Zhu & Chen 1998),

$$F_{\text{int}} \approx \frac{E_{\text{int}}}{\Lambda} \approx \Lambda^2 B_n B_p, \quad (71)$$

where B_n and B_p are the magnetic fields carried by individual vortices and flux tubes, respectively. The force exerted per unit vortex length is

$$f_{\text{pin}} \approx \frac{F_{\text{int}}}{d_p}, \quad (72)$$

where $d_p \approx 95 B_{15}^{-1/2} \text{ fm}$ is the typical distance between flux tubes.

In the unperturbed system, the vortex array is expected to be pinned to the much more numerous flux tubes, but an oscillation with a sufficiently large amplitude may cause large-scale vortex unpinning. In that case, the vortices will be able to move by ‘cutting’ through the flux tubes. In both cases, f_{pin} represents the pinning/interaction force.

The process of cutting is dissipative: part of the fluid’s kinetic energy is transformed into short-wavelength ‘kelvon’ excitations induced along each vortex (see Link 2003 for a discussion). Each kelvon has an effective mass μ , wavenumber k and energy $E_k = \hbar^2 k^2 / 2\mu$. If the relative flux tube–vortex velocity is

$$u_{\text{rel}} = u_p - u_n, \quad (73)$$

then the interaction at each vortex–flux tube intersection lasts a time interval $t_{\text{int}} \sim \Lambda_p / u_{\text{rel}}$. From the uncertainty principle, we also get $E_k \approx \hbar / t_{\text{int}}$ and this leads to

$$k \approx \left(\frac{2\mu}{\hbar \Lambda} u_{\text{rel}} \right)^{1/2} \equiv \frac{1}{\Lambda} \left(\frac{u_{\text{rel}}}{v_{\Lambda}} \right)^{1/2}, \quad (74)$$

where we have defined

$$v_{\Lambda} = \hbar / 2\mu \Lambda \approx 10^9 \text{ cm s}^{-1}. \quad (75)$$

This qualitative analysis is in agreement with the more detailed discussion of Link (2003). Proceeding, we can note that for unpinning to occur, u_{rel} should exceed the fluid velocity lag threshold w_{pin} above which the Magnus force exceeds the pinning force and drives vortex unpinning.⁴ This critical lag is (Link 2003)

$$w_{\text{pin}} \sim \frac{f_{\text{pin}}}{\rho_n \kappa \varpi} \rightarrow w_{\text{pin}} \sim 5 \times 10^5 \rho_{14}^{-1} B_{15}^{1/2} \text{ cm s}^{-1}, \quad (76)$$

⁴ In a state of pinning, $u_n \approx u_p \approx v_p$ and hence the velocity difference appearing in the Magnus force is $u_n - v_n \approx w$.

where $\kappa = h/2m \approx 2 \times 10^{-3} \text{ cm}^2 \text{ s}^{-1}$ is the quantum of circulation for individual vortices (we have also set $\varpi = 10^6 \text{ cm}$ as a representative value for the cylindrical radial coordinate in the outer core). Comparing with equation (25) giving our estimates of the value of fluids' relative velocity excited by the flare event, we see that larger flares can easily satisfy $w_{\text{pin}} < u_{\text{rel}}$, so it would seem that the vortices can indeed unpin.

However, Link's calculation treats the vortex–flux tube intersections as widely separated in relation with the kelvon wavelength, thus ensuring that the excitations do not add up coherently. Mathematically this requirement means that $k d_p \gg 1$, from which we obtain a lower limit on the relative velocity, above which we can trust the damping calculation:

$$u_{\text{low}} \approx 6.5 \times 10^8 B_{15} \text{ cm s}^{-1}. \quad (77)$$

Link's flux tube cutting model would then be valid for $u_{\text{rel}} \gg u_{\text{low}}$. We can see that for magnetar-strong magnetic fields u_{low} is quite large and we should expect $u_{\text{low}} \gg w_{\text{pin}}$. We should also expect that for any reasonable oscillation amplitude, we would have $u_{\text{rel}} \ll u_{\text{low}}$. In other words, a magnetar oscillation capable of forcing vortex unpinning in the first place would be expected to lead to a vortex–flux tube relative velocity somewhere in the range

$$w_{\text{pin}} \lesssim u_{\text{rel}} \lesssim u_{\text{low}}. \quad (78)$$

Unfortunately, this range lies *outside* the validity of Link's flux tube cutting model. For lack of a better alternative, we opt for 'abusing' Link's analysis and *assume* that it remains reliable in the above kinematical range, at least as an order-of-magnitude estimate. This assumption is clearly debatable and this issue should be addressed by more detailed future work. We can note, however, that as long as the kelvon wavelength is microscopically short, $kR \gg 1$ (which is always the case in the relevant parameter range), some dissipation should take place.

The energy penalty for cutting through a single vortex–flux tube intersection is (Link 2003)

$$\Delta E = \frac{2}{\pi} \frac{F_{\text{int}}^2}{\rho_n \kappa} (v_\Lambda u_{\text{rel}})^{-1/2}. \quad (79)$$

The resulting dissipation rate per unit volume can then be written as

$$\mathcal{E}_{\text{cut}} = \frac{\mathcal{N}_n u_{\text{rel}}}{d_p^2} \Delta E, \quad (80)$$

where $\mathcal{N}_n \approx 2\Omega/\kappa$ is the number of vortices per unit area. Combining the previous expressions,

$$\dot{\mathcal{E}}_{\text{cut}} = \frac{4\Omega f_{\text{pin}}^2}{\pi \rho_n \kappa^2} \left(\frac{u_{\text{rel}}}{v_\Lambda} \right)^{1/2}. \quad (81)$$

The next step is to relate the vortex/flux tube velocities with the fluid ones. Based on the high conductivity of the system, we can safely assume that the flux tubes move together with the proton fluid, i.e. $u_p \approx v_p$. It is not so easy to make a similar statement for the vortices and the neutrons. The simplest assumption is to set $u_n \approx v_n$; this could be accurate in the range $u_{\text{rel}} \gg w_{\text{pin}}$ where cutting is strong and the relative motion of vortices is almost that of free vortices. With these identifications, we then have

$$u_{\text{rel}} = \mathbf{w}. \quad (82)$$

The dissipation rate (81) can be also expressed as the work done by the mutual friction force \mathbf{F}_{mf} . To this end, we first consider the drag force per unit vortex length of the general form

$$\mathbf{f}_D = \rho_n \kappa \mathcal{R} u_{\text{rel}}. \quad (83)$$

The (dimensionless) drag coefficient \mathcal{R} is velocity dependent,

$$\mathcal{R} = \mathcal{R}_0 \left(\frac{u_{\text{rel}}}{v_\Lambda} \right)^{-3/2}, \quad (84)$$

and \mathcal{R}_0 is a constant parameter [the $-3/2$ exponent is dictated by equation (86) below].

We can subsequently define the mutual friction force (per unit volume):

$$\mathbf{F}_{\text{mf}} = \mathcal{N}_n \mathbf{f}_D \rightarrow \mathbf{F}_{\text{mf}} = 2\Omega \rho_n \mathcal{R}_0 \left(\frac{u_{\text{rel}}}{v_\Lambda} \right)^{-3/2} u_{\text{rel}}. \quad (85)$$

We then have

$$\dot{\mathcal{E}}_{\text{cut}} = \mathbf{F}_{\text{mf}} \cdot u_{\text{rel}}, \quad (86)$$

which fixes

$$\mathcal{R}_0 = \frac{2}{\pi} \left(\frac{f_{\text{pin}}}{\rho_n \kappa v_\Lambda} \right)^2 \rightarrow \mathcal{R}_0 \approx 10^{-7} B_{15}. \quad (87)$$

The above equations allow the calculation of a mutual friction damping rate

$$\dot{\mathcal{E}}_{\text{fm}} = \int dV \mathbf{F}_{\text{mf}} \cdot u_{\text{rel}} \approx \int dV \mathbf{F}_{\text{mf}} \cdot \mathbf{w}. \quad (88)$$

This becomes (assuming $\rho \approx \text{constant}$)

$$\dot{\mathcal{E}}_{\text{fm}} \approx \frac{16\Omega}{\rho \kappa^2} \frac{f_{\text{pin}}^2}{v_\Lambda^{1/2}} \int_{R_{\text{in}}}^R dr r^2 w^{1/2}, \quad (89)$$

where the radial integral is taken over the region of the outer core.

We can apply the above analysis to the case of magnetar Alfvén oscillations. As we have seen in Section 3.1, we can approximate the mode's kinetic energy as (given the other uncertainties in this calculation, we can ignore the entrainment correction)

$$E_{\text{mode}} \approx \frac{1}{2} \rho_p \int dV w^2 = 2\pi x_p \rho \int_0^R dr r^2 w^2. \quad (90)$$

The mutual friction damping time-scale can be estimated with the help of the standard formula:

$$\tau_{\text{mf}} = \frac{E_{\text{mode}}}{|\dot{\mathcal{E}}_{\text{mf}}|}. \quad (91)$$

From this

$$\tau_{\text{mf}} \approx \frac{\pi \kappa^2 \rho^2 x_p v_\Lambda^2 \int_0^R dr r^2 w^2}{4\Omega f_{\text{pin}}^2 \int_{R_{\text{in}}}^R dr r^2 w^{1/2}}. \quad (92)$$

Given the order-of-magnitude precision of our calculation, we can assume $w \approx \text{uniform}$ and arrive at the simpler result

$$\tau_{\text{mf}} \sim \frac{\pi x_p v_\Lambda^{1/2}}{4\Omega w_{\text{pin}}^2} w^{3/2}, \quad (93)$$

where we have also used (76). This result can be cast in a more transparent form if we express w in terms of the magnetic field perturbation δB . Using equation (24) from Section 3.1, we have

$$\tau_{\text{mf}} \sim \frac{1}{8} x_p P \frac{v_\Lambda^{1/2} v_\Lambda^{3/2}}{w_{\text{pin}}^2} \left(\frac{\delta B}{B} \right)^{3/2}. \quad (94)$$

The key unknown in this expression is the perturbed magnetic field δB . Given that flux tube cutting operates for a mode amplitude above the threshold required by vortex unpinning, it makes sense to normalize δB to its value δB_{pin} , see equation (6) (obviously in the flux tube cutting regime $\delta B > \delta B_{\text{pin}}$).

We can then obtain our ‘final’ result for the mutual friction time-scale,

$$\tau_{\text{mf}} \sim \frac{1}{8} x_p P \left(\frac{v_\Lambda}{w_{\text{pin}}} \right)^{1/2} \left(\frac{\delta B}{\delta B_{\text{pin}}} \right)^{3/2}, \quad (95)$$

$$\approx 3 x_5 \rho_{14}^{-1/2} \left(\frac{P}{10 \text{ s}} \right) \left(\frac{\delta B}{\delta B_{\text{pin}}} \right)^{3/2} B_{15}^{-1/4} \text{ s}. \quad (96)$$

This result implies that a global magnetar oscillation will experience strong damping once the amplitude exceeds the one required for vortex unpinning ($\delta B > \delta B_{\text{pin}}$). The cutting mechanism shuts down for any $\delta B < \delta B_{\text{pin}}$.

4.5 Internal damping: vortex–electron friction

There is a second type of mutual friction operating in our two-fluid system, arising from the dissipative scattering of electrons by the magnetized neutron vortices in the core. In fact, this is the mutual friction mechanism usually considered in the superfluid neutron star literature (see Alpar, Langer & Sauls 1988; Andersson, Sidery & Comer 2006). It corresponds to a force exerted on unit vortex length

$$\mathbf{f}_D = \rho_n \kappa \mathcal{R} (\mathbf{v}_p - \mathbf{u}_n) \quad (97)$$

when the vortex moves with respect to the electrons. Note that the drag coefficient \mathcal{R} appearing in this expression is constant.

Assuming that this is the only frictional force exerted on the vortex, we can arrive at the mutual friction force (for details see Hall & Vinen 1956; Andersson et al. 2006),

$$\mathbf{F}_{\text{mf}} = -2\Omega_n [\mathcal{B} \{\hat{\mathbf{z}} \times (\hat{\mathbf{z}} \times \mathbf{w})\} + \mathcal{B}' (\hat{\mathbf{z}} \times \mathbf{w})], \quad (98)$$

where $\mathcal{B} = \mathcal{R}/(1 + \mathcal{R}^2)$ and $\mathcal{B}' = \mathcal{R}^2/(1 + \mathcal{R}^2)$. The detailed calculation of \mathcal{R} (Alpar et al. 1988; Andersson et al. 2006) suggests that $\mathcal{R} \approx 4 \times 10^{-4}$ and therefore

$$\mathcal{B} \approx \mathcal{R} \ll 1, \quad \mathcal{B}' \approx \mathcal{B}^2 \ll \mathcal{B}. \quad (99)$$

We can estimate the damping time-scale of Alfvén modes as a result of electron mutual friction by following the same logic as in the preceding section. The damping rate is (we note that the \mathcal{B}' -piece of \mathbf{F}_{mf} is not dissipative)

$$\dot{E}_{\text{mf}} \sim 2\Omega\rho\mathcal{B} \int_0^R dr r^2 w^2. \quad (100)$$

This leads to the damping time-scale

$$\tau_{\text{mf}} \sim \frac{1}{2} \frac{x_p P}{\mathcal{B}} \approx 630 x_5 \left(\frac{P}{10 \text{ s}} \right) \left(\frac{4 \times 10^{-4}}{\mathcal{B}} \right) \text{ s}. \quad (101)$$

This is significantly longer than the time-scale associated with flux tube cutting, but short enough to be relevant for the evolution of magnetar QPOs.

As we have pointed out, the derivation of (101) assumes that no other frictional force acts on individual vortices. The vortices in the real system are likely to experience a mutual friction that is a combination of electron friction and of the force due to flux tubes. Both mechanisms operate when the vortices can move with respect to the flux tubes (which are frozen in the proton–electron fluid) and their relative strength would depend on the specific geometry between the vortex and flux tube arrays (see for example Sidery & Alpar 2009). In that case, the mutual friction damping should be given by the shortest time-scale between (96) and (101).

4.6 Internal damping: other mechanisms

The stellar interior allows for additional dissipation channels – the most conventional ones are standard shear and bulk viscosity (these are represented by the viscous force \mathbf{F}_{visc} in the Euler equations of Section 3.1). However, it is easy to see that in the temperature regime where the observed magnetars are expected to reside (i.e. core temperature $T \sim 10^8$ K, see for instance Ho et al. 2012), none of these mechanisms is of any importance. To see this, we can use approximate, back-of-the-envelope, viscous time-scales derived from \mathbf{F}_{visc} as in, for example, Cutler & Lindblom (1987). These are

$$\tau_{\text{sv}} \sim \frac{\rho L^2}{\eta}, \quad \tau_{\text{bv}} \sim \frac{\rho L^2}{\zeta}, \quad (102)$$

where η and ζ are the coefficients of shear and bulk viscosity, respectively. For the former parameter, we use the value appropriate for superfluid matter, associated with electron collisions (Andersson, Comer & Glampedakis 2005) $\eta = 1.6 \times 10^{19} x_5^{3/2} \rho_{14}^{3/2} T_8^{-2}$. For the bulk viscosity coefficient, we use Sawyer’s standard normal-matter formula (Sawyer 1989). (This overestimates the damping rate because it does not account for the suppression of the beta-equilibrium chemical reactions due to neutron and proton superfluidity).

We then obtain

$$\tau_{\text{sv}} \sim 6 \times 10^6 \rho_{14}^{-1/2} x_5^{-3/2} L_6^2 T_8^2 \text{ s}. \quad (103)$$

The bulk viscosity time-scale is even longer so we do not write it explicitly. These results clearly show that neither mechanism is a factor in the evolution of magnetar oscillations.

There is a third possible damping mechanism, most commonly known in the context of the r-mode instability (Andersson & Kokkotas 2001): the viscous boundary layer formed at the base of the crust due to the discontinuity in the mode’s velocity field. This mechanism is rather important for r modes, severely limiting their ‘instability window’ in the temperature regime where neither shear nor bulk viscosity is efficient. However, we can show that the boundary layer poses no threat to magnetar oscillations simply because it is not formed.

This can be deduced by studying a simple plane-parallel model of the crust–core interface (as in Bildsten & Ushomirsky 2000) or by using the results of Mendell (2001). It is then found that the magnetic field can seriously modify the physics of the layer and, among other things, make the layer thicker (in the radial direction). For this to happen, the magnetic field must satisfy $v_A^2/\omega v \gg 1$, where $v = \eta/\rho_p$ and v_A is the superconducting Alfvén speed (7). We find

$$\frac{v_A^2}{v\omega} \sim 10^8 x_5^{-5/2} \rho_{14}^{-3/2} H_{15} B_{15} T_8^2 \left(\frac{100 \text{ Hz}}{f_{\text{mode}}} \right). \quad (104)$$

Clearly, the boundary layer is dominated by the magnetic field. Its thickness is given by (Mendell 2001)

$$\delta_{\text{VBL}} \approx \frac{2v_A^3}{\omega^2 v}. \quad (105)$$

We should obviously have $\delta_{\text{VBL}} \ll R$ for the notion of the layer to make sense. Inserting numbers in this formula,

$$\delta_{\text{VBL}} \sim 10^{14} x_5^{-3} (H_{15} B_{15})^{3/2} T_8^2 \rho_{14}^{-2} \left(\frac{100 \text{ Hz}}{f_{\text{mode}}} \right)^2 \text{ cm}. \quad (106)$$

This length is much bigger than the stellar radius throughout the relevant parameter space. We therefore conclude that a boundary layer does *not* form during magnetar oscillations.

4.7 Gravitational waves: emission and damping

Gravitational wave emission from the excited modes is of interest for two reasons. First, the gravitational waves will themselves damp the oscillations, so we need also to estimate the decay time-scale for gravitational radiation damping. Secondly, the gravitational wave emission may be detectable, and so could provide independent measurements of frequencies and damping times.

Gravitational wave measurements of the damping times would be particularly useful, as the lifetime of the QPOs as observed via X-rays is probably *not* a good indicator of the lifetime of the stellar oscillation itself. This is made clear by the fact that certain QPOs appear briefly only in the *middle* of the X-ray burst, whereas the modes themselves are presumably excited once, at the beginning of the event. Also, the X-ray QPOs are visible as the modulations of the light curve produced by the relativistic fireball created by the initial event, so that once the fireball has faded and the X-ray flux fallen, the X-ray modulations will no longer be detectable, even if the star itself continues to oscillate. The lifetime of the X-ray QPOs should therefore be taken as *lower limits* on the lifetimes of the modes themselves. A ‘direct’ gravitational wave observation of the modes would suffer no such selection effect, and give a robust measure of the mode decay time-scale.

We will begin by estimating the gravitational wave damping time-scale. The modes we consider here are all of low frequency, in the sense of having frequencies well below the dynamical fundamental f-mode frequency of $\sim 1\text{--}2$ kHz. As such, they induce very small density perturbations, consistent with the neglect of such perturbations in Section 3, and to this level of approximation will not radiate mass quadrupole radiation. However, the modes have significant non-zero velocity perturbations, and so there will be mass current quadrupole radiation, the luminosity of which we can easily estimate.

Using the formalism of Thorne (1980), the energy flux for mass current quadrupole radiation is (to order-of-magnitude precision) $\dot{E} \sim (\omega^3 S)^2$, where S denotes the mass current quadrupole, which can be approximated by a simple volume integral over the mass current ρv over the star:

$$S \sim \int |\mathbf{r} \times (\rho \mathbf{v}) r| dV. \quad (107)$$

These will be contributions from both the proton mass current $\rho_p v_p$ and the neutron mass current $\rho_n v_n$.

In the case of Alfvén modes, it is easy to show using the results of Section 3.1 that there is a partial cancellation between the two mass currents, with a net current of $\sim \rho_p v_p m_p^*/m_p$. We can insert this into the equation above for S and then computing the gravitational wave luminosity. Combining with the mode energy of equation (34) leads to a damping time

$$\tau_{\text{GW}} \sim \frac{1}{x_p M R^4 \omega^6} \sim 10^7 x_5^{-1} M_{1.4}^{-1} R_6^{-4} \left(\frac{f_{\text{mode}}}{100 \text{ Hz}} \right)^{-6} \text{ s}. \quad (108)$$

The corresponding time-scale for the damping of crustal oscillations is very similar. Comparing with the various internal and external damping time-scales calculated previously, we see that gravitational radiation is *not* a significant source of damping for our magnetar QPOs.

The detectability of gravitational waves from magnetar flares has already been considered in the literature. Some optimistic upper limits were obtained by looking at how much energy could be channelled into modes (see e.g. Corsi & Owen 2011). Probably more realistically, detailed numerical simulations have also

been performed; see e.g. Zink, Lasky & Kokkotas (2012), who did indeed find excitation of low-frequency modes. A key uncertainty was the damping times of these modes, something which the (short-duration) numerical simulations were unable to compute. Scaling the results of fig. 3 of Zink et al. (2012) to a damping time of, say, 100 s, typical for some of the damping mechanisms considered above, we see that detection by a third-generation detector is possible, and detection by a second-generation (advanced) detector cannot be ruled out, although a large magnetic field strength $\sim 10^{16}$ G would be required.

5 CONCLUDING DISCUSSION

Our three ‘evolutionary pathways’ make several predictions with a bearing on the observational signature of magnetar QPOs. These were discussed in Section 2.2 and can be summarized as follows.

(i) The damping time-scale due to the combined action of superfluid vortex mutual friction and magnetospheric Alfvén flux can move both *up* and *down* during the evolution. The *observed* lifetimes of X-ray QPOs range from tens to hundreds of seconds (Strohmayer & Watts 2006; Hambaryan et al. 2011). Our calculated time-scales can accommodate such a range, although we emphasize that the observed X-ray lifetimes may not accurately reflect the lifetime of the stellar oscillation itself.

(ii) The frequency of the Alfvén spectrum can only be shifted *upwards* to higher frequencies during the evolution as a result of the restoration of neutron superfluidity in the stellar core.

Clearly, our work suggests that analysis of the observational data should allow for the possibility of both frequency and damping time-scale variations for the QPOs. On the theoretical side, our work indicated that a realistic ‘magnetar asteroseismology’ programme should involve many more elements than the mere identification of the observed frequencies with a ‘fixed’ theoretical oscillation spectrum.

Our model can be (and should be) improved in many ways. An obvious missing ingredient is the connection between the oscillation amplitude in the star and that of the emitting region outside the star (the ‘fireball’). Apart from the obvious need of improving the existing magnetar oscillation models, special attention must be given to the damping mechanisms discussed here, i.e. vortex mutual friction and electromagnetic losses into the magnetosphere. Non-linear mode couplings (not considered here) could be an important part of the story too, especially in the early post-flare stages when the mode amplitudes are presumably largest. Another key unknown is that of the initial conditions: which modes are excited and what are their relative amplitudes? Answering these kinds of questions goes hand in hand with understanding the detailed nature of the flare’s trigger mechanism.

On a more technical level, while we were able to confirm the reliability of our simple estimates for the magnetospheric damping time-scales of Sections 4.2 and 4.3, using full-surface integrals for the flux and volume integrals for the mode energy, our estimates for mutual friction damping time-scales of Sections 4.4 and 4.5 were done only in a simpler order-of-magnitude fashion. More detailed calculations, using the full mode eigenfunctions, are needed to test the reliability of our estimates.

Another interesting and novel problem that needs attention concerns computing mode frequencies and damping rates when there are sharp transitions in time and space between superfluid/non-superfluid phases, and between pinned/non-pinned phases. We have provided some simple toy model estimates of how these might tend

to smooth out the transitions between the three regimes of interest to us, but full mode calculations that incorporate such transitions are clearly needed to properly understand this issue.

It is clear that the topical area of magnetar flares is a very challenging one but also one that offers a unique insight into these extreme objects, potentially offering information on both the processes internal to the star and the star's interaction with its magnetosphere.

ACKNOWLEDGEMENTS

It is a pleasure to thank Lars Samuelsson for useful discussions. KG is supported by the Ramón y Cajal Programme of the Spanish Ministerio de Ciencia e Innovación and by the German Science Foundation (DFG) via SFB/TR7. DIJ acknowledges support from STFC via grant number ST/H002359/1, and both authors acknowledge travel support from CompStar (an ESF-funded Research Networking Programme).

REFERENCES

- Alpar M. A., Langer S. A., Sauls J. A., 1988, *ApJ*, 282, 533
 Andersson N., Kokkotas K., 2001, *Int. J. Mod. Phys. D*, 10, 381
 Andersson N., Comer G. L., Glampedakis K., 2005, *Nucl. Phys. A*, 763, 212
 Andersson N., Sidery T., Comer G. L., 2006, *MNRAS*, 368, 162
 Andersson N., Glampedakis K., Haskell B., 2009a, *Phys. Rev. D*, 79, 103009
 Andersson N., Glampedakis K., Samuelsson L., 2009b, *MNRAS*, 396, 894
 Barat C. et al., 1983, *A&A*, 126, 400
 Bildsten L., Ushomirsky G., 2000, *ApJ*, 529, L33
 Blaes O., Blandford R., Goldreich P., Madau P., 1989, *ApJ*, 343, 839
 Cerdá-Durán P., Stergioulas N., Font J. A., 2009, *MNRAS*, 397, 1607
 Chamel N., 2005, *Nucl. Phys. A*, 747, 109
 Chamel N., 2008, *MNRAS*, 388, 737
 Chamel N., 2012, *Phys. Rev. C*, 85, 035801
 Colaiuda A., Beyer H., Kokkotas K. D., 2009, *MNRAS*, 396, 1441
 Colaiuda A., Kokkotas K. D., 2011, *MNRAS*, 414, 3014
 Colaiuda A., Kokkotas K. D., 2012, *MNRAS*, 423, 811
 Corsi A., Owen B. J., 2011, *Phys. Rev. D*, 83, 104014
 Cutler C., Lindblom L., 1987, *ApJ*, 314, 234
 D'Angelo C. R., Watts A. L., 2012, *ApJ*, 751, L41
 Duncan R. C., Thompson C., 1992, *ApJ*, 392, L9
 Duncan R. C., 1998, *ApJ*, 498, L45
 Gabler M., Cerdá-Durán P., Font J. A., Müller E., Stergioulas N., 2011, *MNRAS*, 410, L37
 Gabler M., Cerdá-Durán P., Stergioulas N., Font J. A., Müller E., 2012, *MNRAS*, 421, 2054
 Gabler M., Cerdá-Durán P., Font J. A., Müller E., Stergioulas N., 2013, *MNRAS*, 430, 1811
 Glampedakis K., Andersson N., 2006, *Phys. Rev. D*, 74, 044040
 Glampedakis K., Andersson N., 2011, *ApJ*, 740, L35
 Glampedakis K., Samuelsson L., Andersson N., 2006, *MNRAS*, 371, L74
 Glampedakis K., Andersson N., Samuelsson L., 2011, *MNRAS*, 410, 805
 Goldreich P., Julian W. H., 1969, *ApJ*, 157, 869
 Gusakov M. E., Kantor E. M., 2013, *MNRAS*, 428, L26
 Hall H. E., Vinen W. F., 1956, *Proc. R. Soc. Lond. A*, 238, 215
 Hambaryan V., Neuhäuser R., Kokkotas K. D., 2011, *A&A*, 528, A45
 Haskell B., Glampedakis K., Andersson N., 2013, preprint ([arXiv:1307.0985](https://arxiv.org/abs/1307.0985))
 Ho W. C. G., Lai D., 2000, *ApJ*, 543, 386
 Ho W. C. G., Glampedakis K., Andersson N., 2012, *MNRAS*, 422, 2632
 Horowitz C. J., Kadau K., 2009, *Phys. Rev. Lett.*, 102, 191102
 Israel G. L. et al., 2005, *ApJ*, 628, L53
 Lander S. K., Jones D. I., 2011, *MNRAS*, 412, 1730
 Levin Y., 2006, *MNRAS*, 368, L35
 Levin Y., 2007, *MNRAS*, 377, 159
 Link B., 2003, *Phys. Rev. Lett.*, 91, 101101
 Mendell G., 1991, *ApJ*, 380, 515–530
 Mendell G., 2001, *Phys. Rev. D*, 64, 044009
 Messios N., Papadopoulos D. B., Stergioulas N., 2001, *MNRAS*, 328, 1161
 Passamonti A., Lander S. K., 2013, *MNRAS*, 429, 767 and preprint ([arXiv:1307.3210](https://arxiv.org/abs/1307.3210))
 Piro A. L., 2005, *ApJ*, 634, L153
 Prix R., 2004, *Phys. Rev. D*, 69, 043001
 Ruderman M., Zhu T., Chen K., 1998, *ApJ*, 492, 267
 Samuelsson L., Andersson N., 2007, *MNRAS*, 374, 256
 Sauls J. A., 1989, in Ogelman H., van de Heuvel E. P. J., eds, *Timing Neutron stars*. Kluwer, Dordrecht, p. 457
 Sawyer R. F., 1989, *Phys. Rev. D*, 39, 3804
 Sidery T., Alpar M. A., 2009, *MNRAS*, 400, 1859
 Sotani H., Kokkotas K. D., Stergioulas N., 2008, *MNRAS*, 385, L5
 Strohmayer T. E., Watts A. L., 2005, *ApJ*, 632, L111
 Strohmayer T. E., Watts A. L., 2006, *ApJ*, 653, 593
 Thompson C., Blaes O., 1998, *Phys. Rev. D*, 57, 3219
 Thompson C., Duncan R. C., 1995, *MNRAS*, 275, 255
 Thompson C., Duncan R. C., 2001, *ApJ*, 561, 980
 Thorne K. S., 1980, *Rev. Mod. Phys.*, 52, 299
 Tilley D. R., Tilley J., 1990, *Superfluidity and Superconductivity*. IoP Publishing, Bristol, UK
 van Hoven M., Levin Y., 2008, *MNRAS*, 391, 283
 Watts A. L., Strohmayer T. E., 2006, *ApJ*, 637, L117
 Woods P. M., Thompson C., 2004, in Lewin W. H. G., Van der Klis M., eds, *Compact Stellar X-ray Sources*. Cambridge Univ. Press, Cambridge
 Zink B., Lasky P. D., Kokkotas K. D., 2012, *Phys. Rev. D*, 85, 024030

This paper has been typeset from a $\text{\TeX}/\text{\LaTeX}$ file prepared by the author.